An Algorithm for Shrinking Blood Receptacles using Retinal Internal Pictures for Clinical Characteristics Measurement

Aws A. Abdulsahib[1], Moamin A Mahmoud[2]*, Sally A. Al-Hasnawi[3]

College of Graduate Studies, Universiti Tenaga Nasional, Selangor, Malaysia[1]
The Institute of Informatics and Computing in Energy, De-partment of Computing[2]
College of Computing and informatics, Universiti Tenaga Nasional, Selangor, Malaysia[2]
BIOCORE Research Group, Faculty of Information & Communication Technology, Al-Farahidi University, Baghdad, Iraq[3]

Abstract—**The manual technique that might use for shrinking vessels blood in the retinal fundus images has significant limitations, such as the high rate of time consumption and the possibility of human error, precisely appear with the sophisticated structure of the blood receptacle and a hung amount of the retinal fundus photograph that needs to be anatomic. Moreover, the automatic proposed algorithm that will utilize shrinking and explore helpful clinical characteristics from retinal fundus photographs in order to lead the eye caregiver to early diagnosis for various retinal disorders and therapy evaluations. A precise, quick, and fully-automatic algorithm for shrinking blood receptacles and clinical characteristics measuring technique for internal retinal pictures is suggested in order to increase the diagnostic accuracy and reduce the ophthalmologist's burden. The proposed algorithm's main pipeline consists of two fundamental stages: picture shrinkage and medical feature elicitation. Many exhaustive practices were conducted to evaluate the efficacy of the sophisticated fully-automated shrinkage system in figuring out retinal blood receptacles using the DRIVE and HRF datasets of exceedingly demanding fundus images. Initially, the accuracy of the created algorithm was tested based on its ability to accurately recognize the retinal structure of blood receptacles. In these attempts, several quantitative performance measures precisely five were computed to validate the efficacy of the exact algorithm, including accuracy (Acc.), sensitivity (Sen.), specificity (Spe.), positive prediction value (PPV), and negative prediction value (NPV). When contrast with modern receptacles shrinking approaches on the DRIVE dataset, the produced results have enormously improved by obtaining accuracy, sensitivity, specificity, positive predictive value, and negative predictive value of 98.78%, 98.32%, 97.23%, and 90. Based on five quantitative performance indicators, the HRF dataset led to the following results: 98.76%, 98.87%, 99.17%, 96.88%, and 100%.**

Keywords—*Segmentation vessels / shrinking blood receptacles; clinical characteristics measurement; internal pictures for retinal; morphological filtering algorithm*

I. INTRODUCTION

Direct ophthalmoscope, or manual examination of the internal photograph by a professional, is being replaced by a computer-attribution diagnosis of retinal internal images. Furthermore, the computer-attribution diagnosis of retinal internal pictures is as accurate as a direct ophthalmoscope and requires less processing and analysis time. Retinal fundus pictures are commonly used to diagnose many eye-related illnesses that lead to vision loss, for instance, diabetic retinopathy in addition to macular degeneration [1]. The extraction of retinal blood vessels from fundus pictures is one of the essential processes in detecting diabetic retinopathy. Even though numerous segmentation approaches have been proposed, segmentation of the retinal vascular network and picture quality remains difficult. Noise (typically owing to uneven lighting) and narrow vessels are now critical obstacles in retinal vascular segmentation. Additionally, most of the proposed segmentation algorithms optimize the preprocessing and blood receptacle seg-mentation subjects for each dataset separately. As a result, these algorithms can typically reach a high rate of accuracy for the optimized dataset, but their accuracy will be lowered when applied to different datasets. Although most vessel segmentation methods include pretreatment procedures to improve vessel appearance, other plans skip the preprocessing steps and jump straight to the segmentation stage [2].

Blood receptacle segmentation is an essential required step to do the quantitative investigation of retinal photographs, where a set of critically beneficial clinical features such as the tortuosity, length, density, and thickness, of the blood vessel can be extracted from the segmented vascular tree. Furthermore, the segmented vascular tree has also been used in several medical applications, including retinal image mosaic structure, temporary and/or multi-modal image registration, optic disc identification, biometric identification, and fovea localization. Many segmentation approaches nowadays use machine learning ideas in conjunction with traditional techniques to improve segmentation accuracy by providing a statistical analysis of data to enhance segmentation algorithms [3]. Based on the usage of labeled training data, these machine learning principles can be divided into unsupervised and supervised approaches. In a supervised technique, a human operator labels and select a class for every single pixel in the internal picture, such as vessel and non-vessel. A classifier is trained using the tags supplied to the input. A sequence of characteristics vectors is formed from the data being processed (pixel-wise characteristics in picture segmentation defects). Similar samples are grouped into various classes using predetermined characteristics vectors

*Corresponding Author.

that are distinguished without any labels in an unsupervised technique. This accumulating is dependent on several assumptions about the input dataset structure, namely that there are two kinds of classes of the input dataset with identical characteristics vectors (blood receptacle and not blood receptacle). Depending on the situation, this matching metric might be sophisticated or specified by a basic metric like pixel contrasts [4].

The analysis of the blood receptacle tree in internal images with precision and accuracy can provide several essential aspects for diagnosing various retinal disorders. However, when utilized as the first step which is represented by preprocessing for higher-level picture detection, retinal blood vessel segmentation might significantly impact other applications. For instance, reliable blood vessel tree detection might be employed in recording time series internal images, finding the optical disc or over, recognizing the retinal blood receptacle fiber layer, and biometric identification. There is a substantial amount of work on this topic due to the applications wide range and the fact that shrinkage of retinal blood receptacles is one of the critical jobs in retinal picture processing [5].

To increase diagnosis precision and reduce ophthalmologists' burden, an accurate, quick, and totally automatic blood receptacle shrinking and clinical characteristics measuring algorithm for retinal internal pictures is presented. The proposed algorithm's main pipeline consists of two critical stages: picture segmentation and clinical feature extraction. In the segmentation stage, a fully automated segmentation method called a morphological filtering algorithm addressed by MFA is used to find blood receptacles in retinal photographs.

In the morphological filtering algorithm, an efficient and reliable image pre-processing procedure is applied to preserve the vessel's structure and eliminate the noise level using the Anisotropic Diffusion (AD) filtering and Gaussian filtering, respectively. This is followed by removing all undesired objects (e.g., small vessel segments) in the enhanced image by applying morphological operations. Finally, all the retinal blood vessels are detected by utilizing an efficient edge algorithm based on efficient filter which is an improved Canny edge detector. Finally, the output segmented images produced from the proposed segmentation algorithm is fused to produce the final segmented image. In the post-processing step, a novel blood vessel linking procedure is proposed to correctly join the discontinuous blood vessels produced in the segmented picture resulting from the fusing stage. In the clinical features extraction stage, several helpful clinical characteristics are computed, for instance the tortuosity, thickness, density, and length of the blood vessel, which are efficiently used in the early diagnosis of several cardiovascular and ophthalmologic diseases. In this stage, an efficient and accurate algorithm for computing the blood vessel thickness is proposed. The main contributions list can be summarized as follows:

- An accurate, quick, and fully-automated blood vessels shrinkage and clinical characteristics assessment

algorithm is suggested to improve diagnosis precision and reduce ophthalmologists' burden.

- Fully-automated segmentation algorithm is proposed and named as a morphological filtering algorithm to accurately detect the blood vessels in the retinal images.

- A novel blood vessel linking procedure is proposed to correctly join the discontinuous blood vessels produced in the segmented image resulting from the previous step.

- This research considers as a second stage from our main goal by developing a fully automated and real-time retinal blood vessels hybrid segmentation and clinical features extraction model in fundus images and for the first stage represented by trainable filter algorithm that already completed successfully.[6].

- The rest zone of this study is consist of Section II which presented a related works on Blood receptacles shrinking and medical feature measuring algorithm for internal pictures of the retina Section III outlines the major processes of the proposed morphological filtering algorithm, which consists of three primary stages: image preprocessing, morphological operations, and vessel recognition. Several comprehensive tests were undertaken to evaluate the performance and accuracy of the newly created fully-automated shrinkage system for analyzing retinal blood receptacles through utilizing two difficult internal binary photograph datasets, as described in Section IV in addition to Section V discusses the outcome results and future work as a final topic.

II. RELATED WORK

The shrink in the retinal internal image is considered as a first stage concerned with identifying the several diseases that related to the eyes. In general, blood receptacles look like a structure tree. Morphological characteristics includes width, length plus to branching of the eye, and others play an enormous part in detecting and treating various of eyes diseases, according to work published by [5] Classification of microaneurysms and non-macro aneurysms is a concern using morphological filters algorithm to detect diabetic retinopathy in retinal vessels images by utilizing the evaluation matric such as accuracy, sensitivity, and specificity. In addition, the study did the experiments using the IDRiD dataset with an average result of 80.85%. Thus, its notice some limitations in their proposed methods summarized by resolution point need to be more enhancement. They have used only one dataset in the whole of the experiments. According to S. Annand et al. [7] they are working on Optic disc analysis in retinal blood vessels in the fundus using contourlet sub-bands, superimposed edges with morphological filling through several kinds of datasets, including DRIVE, STARE, MESSIDOR, etc. E-aphtha, Diaretdb1. Moreover, the utilized dataset highlights the accuracy channel that registers 97.15% output result even though the outcome is high. Still, there are some points it needs to be enhance, such as the datasets that are used with significant numbers of users lead to have the

configuration complexity that might happen between the various datasets and the proposed methods. Another work by [8], the study proposed the domain of Retinal Vessel Segmentation in Diabetic Retinopathy Using a Morphological Top Approach in medical Images by implementing two types of data: HAGIS and HRF, which succeed by achieving 95.12%, 94.37%, respectively. Several disorders may be impacted by a particular segmentation procedure, resulting in limits because there are numerous types of diseases, for instance glaucoma, age macular degeneration, hypertension, that conceder harmful and significantly affect the patient's health.

In [9], the work on the execution analysis of auto-detection of diabetic retinopathy utilizing the proposed operation algorithms with the same concept of evaluation matric but with a deferent dataset named by DIARETDB1 to achieve a 98.68% percentage. At some point, the computational timing is quite long, based on several observations. Another study by [10], its introduced analyses of retinal blood receptacle from eyes scope images through utilize morphological method implemented through DRIVE, HRF dataset to extract the Acc., Sen., and Spe. with the exact result of the accuracy is 0.9541,0.9478 respectively. Therefore, there are some misclassified structures, such as vessels giving poor segmentation output. Also, U. Ozkaya et al. [11] presented the efficiency of retinal blood receptacle shrink utilizing morphological operations using DRIVE dataset to achieve 95.61% with some limitations of the proposed methods that do not diagnose critical diseases such as hypertension and diabetic retinopathy. Charu Bhardwaj et al. [12] focusing on the execution analysis of retinal characteristics for diabetic retinopathy characterization and diagnoses by using DRIVE, STARE to extract the evaluation matric category that is divided into three types starting by accuracy and end with specifically to highlight the accuracy average result 95.50%, 94.80% respectively. However, it needs to be more accurate to positively match the manual segmentation results. In this paper, we emphasize the morphological filter algorithm that was modified using a very powerful and common dataset, DRIVE and HRF, for accurate, quick, and full-automatic blood receptacle shrink and clinical characteristics. A measurement approach for retinal internal pictures is presented to enhance or develop diagnostic quality and reduce ophthalmologists' effort.

III. PROPOSED AUTOMATIC BLOOD VESSELS SEGMENTATION AND CLINICAL FEATURE MEASUREMENT ALGORITHM

The quantitative investigation of retinal images is widely utilized for rapid detection, observation, and treatment assessment of cardiovascular and ophthalmologic diseases, for instance, macular degeneration, eyes diabetes, glaucoma, hypertension, arterio-sclerosis, vein occlusion, and choroidal neovascularization. Among these mentioned diseases, diabetic retinopathy and macular degeneration are considered the two main reasons for blindness. Blood receptacle shrink is an essential stage required for the quantitative investigation of retinal photographs, where a set of critically beneficial medical characteristics for instance the density, tortuosity, length, and thickness, of the blood vessel, can be extracted

from the segmented vascular tree. Furthermore, the segmented vascular tree has also been used in several medical applications, including retinal image mosaic structure, temporary and/or multi-modal image registration, optic disc identification, biometric identification, and fovea localization. Accordingly, it is hypothesized that an autonomous method for segmenting and extracting valuable clinical information from retinal blood vessels will aid ophthalmologists and eye specialists in the early diagnosis of various retinal illnesses and the evaluation of treatment options. Fig. 1 shows the projected blood vessel segmentation and clinical features measurement.
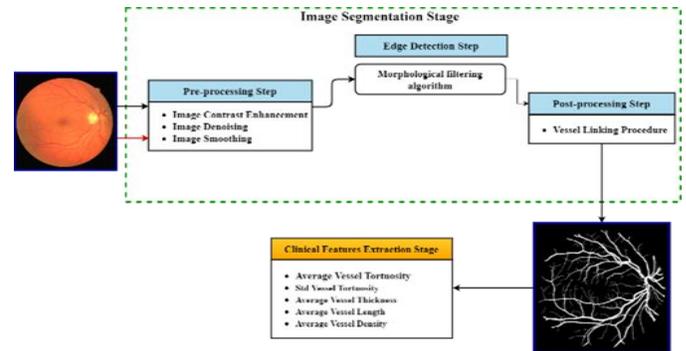
Fig. 1. Diagram of the Proposed Blood Receptacles Shrink and Clinical Features Measurement Algorithm.

A. The Morphological Filter Algorithm

As we presented in Fig. 2 the main steps of the morphological filtering algorithm, which is composed of three main stages, including the image pre-processing stage, the morphological operations stage, and the vessels detection stage. In the image pre-processing step, the AD filtering and Gaussian filtering are applied on top of the extracted green channel of the retinal image to enhance edges' structures and eliminate the noise in the retinal fundus image, respectively. Then, a set of morphological operations are applied on top of the enhanced image produced from the previous stage to discard the background and all the unwanted objects (e.g., small vessel segments). Finally, the retinal blood vessels are detected by utilizing an efficient edge detection algorithm based on edge detector filter addressed by an improved Canny edge detector. The main steps of the selected filter are explained in detail in the next sub-sections.
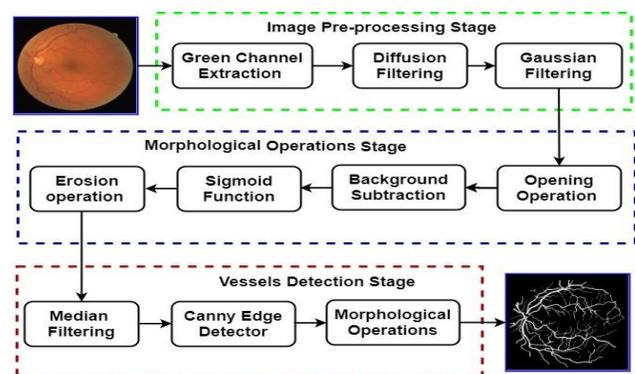
Fig. 2. The Fundamental Stages of the Proposed Morphological Filtering Algorithm for Detecting the Retinal Blood Vessels.

1) Image pre-processing stage: In this stage, the crucial aim is to improve the non-uniform illumination, controlling the contrast of the retinal picture and de-creasing the background noise. The main steps of the proposed image pre-processing can be summarized as follows:

a) Extracting the best channel which is the green from the colored retinal internal photograph.

b) Correcting the non-uniform illumination and enhancing the visibility of the edges' tree structures in the retinal internal picture by using AD filter.

c) Applying the 2D Gaussian filter to smooth the retinal image and eliminate the background noise.

Despite of the human observer can efficiently identify the blood vessel structures using the full-color image, however, processing the three channels of the input image can increase the computational complexity of the proposed algorithm where a long time will be required to deliver the final segmented image. Thus, the proposed morphological filtering algorithm starts with extracting the green channel of the input picture because it gives a better distinction between the background layer and the retinal blood receptacle than other channels, as shown in Fig. 3.
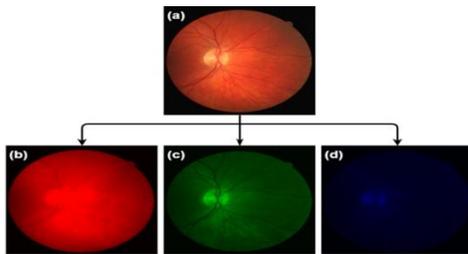
Fig. 3. The Three Channels of the Coloured Retinal Image: (a) Main Picture, (b) Red Conduit Picture, (c) Green Conduit Picture, and (d) Blue Conduit Picture.

In most cases, the retinal images have some background pixels with intensity values similar to the lighter pixels of the retinal blood vessels. These pixels can significantly degrade the outcome of the proposed segmentation algorithm. Therefore, the AD filter [13] was used to the green conduit of the retinal picture after rescaling it to the range of [0, 1], to correct the non-uniform illumination and enhance edges' structures in the retinal picture, as presented in Fig. 3(b). The AD filter can be represented as follows:

$$I_{i,j}^{t+1} = I_{i,j}^t + \lambda[c_N \cdot \nabla_N I + c_S \cdot \nabla_S I + c_E \cdot \nabla_E I + c_W \cdot \nabla_W I]_{i,j}^t \qquad (1)$$

Here, I refer to the retinal image, $0 \leq \lambda \leq 1/4$, The (c) parameter represents the conduction coefficients which is updated every iteration as a brightness gradient function, (t) represents the iteration index, and (∇) refers to the nearest neighbour variances in all the directions N, S, E, and W, as bellows:

$$\nabla_N I_{i,j} = I_{i-1,j} - I_{i,j}$$

$$\nabla_S I_{i,j} = I_{i+1,j} - I_{i,j}$$

$$\nabla_E I_{i,j} = I_{i,j+1} - I_{i,j}$$

$$\nabla_W I_{i,j} = I_{i,j-1} - I_{i,j} \qquad (2)$$

In this work, these values of the λ and t parameters are set to 0.20 and 5, respectively. This was followed by applying the 2D Gaussian filter to assure the smoothness in the retinal internal picture in addition to eliminating the background noise, as presented in Fig. 3(c). The 2D Gaussian filter is distinguished by a non-uniform low-pass filter, whose 2D filter coefficients are computed as follows:

$$G(x, y) = \frac{1}{2\pi\sigma^2} e^{-\frac{x^2+y^2}{2\sigma^2}} \qquad (3)$$

Here, the (x, y) refers to the filter center, and σ refers to (SD) Standard Deviation of the Gaussian filter.

2) Morphological operation stage: Typically, morphological operations can be employed to accurately extract the image's components, which are proven to be extremely helpful for interpreting and representing the different shapes that exist inside the input image rather than pixels' intensities, such as borders, skeletons, and convex hulls [14]. The morphological operations are considered powerful tools that can be efficiently employed in solving several tasks in image processing. Dilation, erosion, opening, closing, bottom-hat, and top-hat transformation are the fundamental morphological operations that can be utilized to segment, manipulate and adjust the objects shown in the input image depending on their structure [15]. In general, these morphological operations were only applied to the binary images, and then they were extended to process the grey-scale images as well. The primary aim of this stage is to define the vessels' structure precisely by eliminating the defects, such as various kinds of noise that can influence the blood vessels' structure and produce more visible structures of the blood vessels. The main stages in the selected morphological operations stage are implemented sequentially as follows:

a) Applying the opening operation with a disk structure element of 3 pixels.

b) A background subtraction procedure was implemented to split the foreground objects from the image's background.

c) A sigmoid function was employed to decrease the effect of the non-uniform illumination of the retinal pictures.

d) Improving the appearance of the retinal blood receptacles by applying the erosion process.

In this stage, two different morphological operations were applied, namely the opening and erosion operations. The morphological operations were further employed in other steps of the proposed blood vessel segmentation algorithm to exclude the unwanted features (e.g., small vessel parts) without changing the main structure of the blood vessel. Usually, the morphological operations take two different parameters, including the picture that needs to be processed. The shape in addition to size of the tree structure element plays a significant role in detecting a feature representation of a given size and shape in the input image. Thus, the size and shape of the structuring element are selected according to the demand and purpose of the adopted application. The erosion

and dilation operations are the essential morphological operations utilized to lessen and boost the objects in the image, respectively. The erosion and dilation operations are defined as follows.

$$f \, \Theta \, B = \min_{u,v}\left(f_{(x+u,y+v)} - B_{(u,v)}\right) \qquad (4)$$

$$f \oplus B = \max_{u,v}\left(f_{(x-u,y-v)} + B_{(u,v)}\right) \qquad (5)$$

where (f) represents a greyscale image B refers to the structuring element. $f \, \Theta \, B$ and $f \oplus B$ represent erosion and dilation, respectively. Morphological opening operation is applied to delete undesired precise structures in the input picture by implementing an erosion procedure followed by a dilation process. In contrast, a morphological closing operation is applied to fill or merge some structures in the input picture by implementing the dilation procedure followed by the erosion process. The morphological opening and closing operations can be defined as follows:

$$foB = (f \, \Theta \, B) \oplus B \qquad (6)$$

$$f \bullet B = (f \oplus B) \Theta \, B \qquad (7)$$

In this stage, several kinds of experiments were conducted to select the methods of applied in this stage using retinal fundus images with various levels of noise and lighting conditions. The main aim here is to improve the structure of blood vessels without missing essential characteristics in the retinal picture. In the current stage, the opening operation was applied to the enhanced image produced from the prior stage by employing an optic disk element of 3 pixels. Then, a subtraction procedure for the background layer was implemented to split the foreground objects from the image's background and identify the retinal blood vessels accurately. Next, a simple image contrast enhancement process using a sigmoid function [16] is implemented as follows:

$$g(x,y) = \frac{1}{1+e^{\left(c*(Th-f(x,y))\right)}} \qquad (8)$$

Where f and g of (x,y) is the input and the enhanced photograph. Herein, the contrast parameter (c), and the Threshold parameter (Th), are empirically chosen to be 4 and 0.5, respectively. The main advantage of this step is to decrease the impact of the non-uniform illumination by narrowing in addition to extending the values range of the bright and dark pixels in the retinal photograph, sequentially. Finally, the erosion process was also applied by employing a structural element of 2-pixels to improve the appearance of the retinal blood vessels, as presented in Fig. 3(d). Undesired segments of one-pixel size were excluded.

3) Vessel's detection stage: The vessels detection procedure was applied to preserve beneficial structural details of the blood vessels' borders and to carefully discard the unwanted objects. As depicted in Fig. 4, the fundamental steps of the selected vessels detection process might be outlined as follows:

a) Eliminating the noise level produced from the morphological operations stage by applying the median filter.

b) An improved Canny edge detector was employed to accurately identify the blood vessels.

c) A refinement vessel's structure procedure based on applying a set of morphological operations was implemented to maintain the actual thickness of the detected blood vessels and to eliminate unwanted objects in the segmented image.

Initially, the median filter was applied to eliminate the noise produced from the morphological operations stage that can significantly influence the precision of the blood vessels detection in the later steps. The median approach is a non-linear method that is utilized to eliminate the noise from a given image to enhance the outcomes of subsequent processing (e.g., the edge detection process in an image). The median filter is very widely applied in addressing several image processing problems due to its ability in preserving the edges and removing noise. In this work, a media filter of size (5×5) pixels.

The blood vessels were then identified by using an improved Canny edge detector. First, the Gaussian filter was applied to further decrease the noise level in the picture. This was followed by calculating the gradient magnitude along with its vectors for each pixel of the enhanced image. An algorithm of non-maxima suppression was later implemented by utilizing the gradient magnitude and direction to be recognized and assigned as a border pixel by employing the thresholding approach. The main stimulus for applying the improved Canny edges detector is to accomplish some beneficial characteristics, including reducing the possibility of duplicated responses to a singular edge; reducing the likelihood of neglected edges; reducing the distance computed between the pixels of the identified edges and the original edges. These four characteristics might conceder as a critical role in solving the problems of detecting retinal blood receptacles precisely. The main steps of applying the improved Canny edges detector can be summarized as follows:

1) Smooth Image: Reducing the noise and smoothing the retinal image by applying the Gaussian filter. Suppose $G(x,y)$ represents the Gaussian filter as revealed in Eq. (9) and $I(x,y)$ represents the retinal image. Then the smoothed image can be obtained by convoluting I with G of (x,y) as follows:

$$S(x,y) = G(x,y) \otimes I(x,y) \qquad (9)$$

2) Gradient Magnitude: Computing the gradient magnitude of the smoothed image $S(x,y)$ is utilized to compute the variation value of (G_X) and (G_Y), sequentially, same as below:

$$G_X(x,y) \approx$$
$$[S(x,y+1) - S(x,y) + S(x+1,y+1) - S(x+1,y)]/2 \quad (10)$$

$$G_Y(x,y) \approx$$
$$[S(x,y) - S(x+1,y) + S(x,y+1) - S(x+1,y+1)]/2 \quad (11)$$

From Eq. (10) and (11), the gradient magnitude and its direction are computed, respectively, as in Eq. (12) and (13):

$$G(x,y) = \sqrt{G_X^2(x,y) + G_Y^2(x,y)} \qquad (12)$$

$$\theta(x,y) = tan^{-1}\left(\frac{G_Y^2(x,y)}{G_X^2(x,y)}\right) \qquad (13)$$

3) Non-maxima Suppression Algorithm: The computed gradient magnitude usually includes extended ridges nearby the local maximum. Thus, the non-maxima suppression algorithm was applied to thin these extended ridges. A gradient vector (di) composed of four discrete directions (e.g., horizontal, vertical, 45° and - 45°) is computed for each pixel (x, y) of the normal edge. Then the closest direction to $\boldsymbol{\theta(x,y)}$ is defined from these four directions. If the value of gradient magnitude $\boldsymbol{G(x,y)}$ was lower than the vectors (di), then the non-maxima algorithm is equal to zero (suppression); else, N (x, y) = $\boldsymbol{G(x,y)}$.

4) Hysteresis Thresholding Algorithm: This algorithm is applied to detect and connect the pixels of the actual edges.

In most cases, thresholding the input image can produce several false detected edges. To decrease the rate of false detected edges, a thresholding algorithm can be applied using two different threshold values, named the low threshold (TL) and the high threshold (TH). It defines the non-maxima approach NH (x, y) after hysteresis thresholding N (x, y) using the high threshold (TH) and defines the non-maxima approach NL (x, y) after the method of thresholding using the low threshold (TL). Obviously, the NH (x, y) has the stronger edge representations compared with the NL (x, y) which contains the weaker edge representations.

After the improved Canny edge detector has applied, a refinement vessel's structure procedure was implemented to maintain the actual thickness of the detected blood vessels and to eliminate some unwanted objects in the segmented image. This refinement procedure starts by applying the dilation process by employing two line-formed structural elements of three pixels with angles between 90° and 0°, sequentially. Then, the erosion process was implemented by employing a structural element of one pixel to sharpen the edges of the defined blood vessels. Finally, all the objects of an overall area of fewer than 100 pixels were discarded from the final segmented image, as shown in Fig. 4(e).
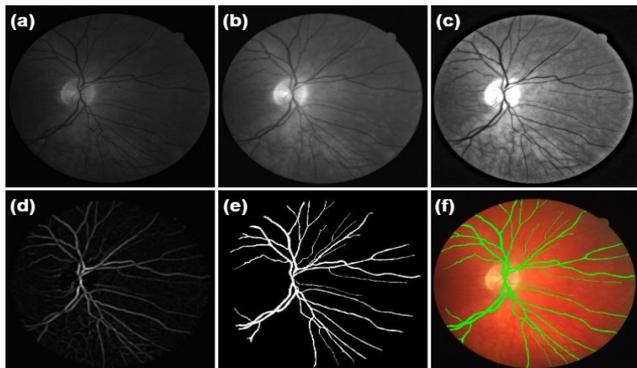
Fig. 4. The Proposed Morphological Filtering Algorithm Outputs: (a) Normalized Green Conduit, (b) AD Output, (c) Gaussian Filtering Output, (d) The Output of the Morphological Operations Stage, (e) The Final Output of the Edge Detection Stage, (f) The Overlapped Automated Segmented Image with the Original Retinal Image.

B. Post-Processing Stage

Once, the segmented retinal image is obtained from the morphological, the output is used to produce the final segmented image. Then, a novel blood vessel linking procedure was proposed to correctly join the discontinuous blood vessels produced in the segmented image resulting from the previous step. These discontinuous blood vessels are presented in the eventual segmented picture due to poor visibility of the specific portions of blood vessels or the noise presented in the retinal image. The accuracy of the extract clinical characteristics, for instance, the thickness, length, density, and tortuosity of the blood vessel can significantly be affected by the appearance of the discontinuous blood vessels. Thus, a new process was selected in this study to correctly join the discontinuous blood vessels in the final segmented photograph. The proposed blood vessel linking procedure was implemented as follows:

1) Producing the skeleton blood vessels structure of the final retinal segmented image, and then identifying the vessels' end-points.

2) Defining a possible highest distance between the endings of each two segments of a disconnected blood vessel. Then a circular-shaped structure element of radius = (highest distance)/2 was placed at the end of each blood vessel. If the ends of the two blood vessels were approaching each other, then the placed structural elements were overlapped, as displayed in Fig. 5(c).

3) Finally, the thinning process was applied to the whole image. Hence, a line of one pixel wide will be left by the thinned structural elements to link the two endings of the vessel. While, the separated ends are recovered to their initial structure, as displayed in Fig. 5(d).
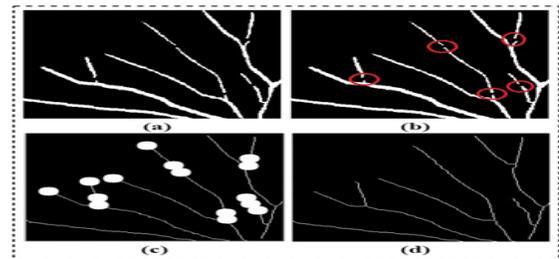
Fig. 5. The Proposed Blood Vessel Linking Procedure: (a) The Segmented Blood Vessel Structures, (b) The Disconnected Blood Vessels Marked in the Red Circles, (c) The Binary Circular-shaped Structural Elements are Drawn at the Ends of each Blood Vessel Segment, and (d) The Resulting Image with Linked Blood Vessels.

C. Clinical Feature Extraction Stage

The abnormalities in the retinal blood vessel structures, including the morphologic modifications in vessel tortuosity, shape, thickness, and length might be connected to the existence of cardiovascular and eye diseases. Therefore, the automatic quantitative analysis process of abnormalities in blood vessel structures can be extremely useful to help ophthalmologists and eye specialists in the early diagnosis of different retinopathies diseases, describe their severity level, and treatment assessments .One of the main aims of this work is to develop an automated morphologic description procedure

to analyze the whole blood vessel network in the retinal image. The clinical features extraction stage computes a set of useful clinical features from the automatically detected retinal blood receptacle in an accurate path. In the current stage, a number of morphological clinical features associated with the healthiness of the retinal blood receptacles are extracted as follows:

1) Vessel's length: The length of the retinal blood vessel was computed for each vessel's segment by firstly taking the vessel's skeleton structure, and then the distance between sequential pixels in the blood vessel segment is summed as in Eq. (14).

$$Vessel\ Lengh = \sum_{i=1}^{N-1} \sqrt{(x_{i-1} - x_i)^2 + (y_{i-1} - y_i)^2} \quad (14)$$

Here, (N) refers to the number of sequential pixels produced from the blood vessel skeleton part, with (x_i, y_i) refers to the pixel's coordinates in the blood vessel part.

2) Vessel density: The retinal blood vessels density was calculated by dividing the sum of all the pixels in the blood receptacles by overall area of the whole retinal image as shown in Eq. (15):

$$Vessel\ Density = \frac{\sum The\ vessel\ pixels}{ImageArea\ (mm^2)} \quad (15)$$

3) Vessel tortuosity: The tortuosity coefficient of the blood vessel is interpreted as a degree of twists presented in the blood receptacle course, as shown in Fig. 6. Some studies have proved that the vessel tortuosity coefficient can be linked with the average fundus blood pressure, however, no significant increase was observed until the critical blood pressure level is reached [17, 18]. Herein, the mean tortuosity coefficient of the whole retinal blood vessel network was computed. First, the skeleton structure of the blood vessels was produced. This was followed by defining the branch points of the blood vessels to divide the length of Blood Vessel Segment (BVS) into (b) branches as in Eq. (16):

$$BVS = s_1 + s_2 + \cdots + s_b \quad (16)$$

Then, the tortuosity coefficient index for the (BVS) was then computed as follows:

$$TC(BVS) = \sum_{n=1}^{b} {s_{length}(n)}\Big/{s_{straight}(n)} \quad (17)$$

Fig. 6.   An Example of Severe Retinal Blood Vessel Tortuosity is a Patient with Severe Non-proliferative (NPDR) Disease [19].

where s_{length} refers to the length of the vessel branch, and it was estimated by Eq. (14). $s_{straight}$ is the straight distance between the endings point and was estimated as follows?

$$s_{straight} = \sqrt{(x_N - x_1)^2 + (y_N - y_1)^2} \quad (18)$$

Here, (N) refers to the specific number of essential subjects captured from the sub branch of the blood vessels. While (x, y) refers to the pixel's coordinates in each branch of the blood vessels. Finally, the mean tortuosity coefficient of the entire blood vessels network was acquired by calculating the mean tortuosity values obtained of each blood vessel.

4) Vessel thickness: The blood vessel thickness is referred to as the average width of the retinal blood vessels. In this PhD thesis, a new procedure for computing the retinal blood vessel thickness is developed. Fig. 7 presents the outcome results of the enhanced thickness procedure. The primary steps of the developed procedure after identifying each blood vessel were implemented as below:

a) Distance transformation was computed from the photograph of detected retinal blood vessels, where all background pixels in the transformed image become white, while the object pixels become black. This transform calculates the Euclidean distance for each black pixel in the segmented image to the nearest non-zero pixel. In the developed procedure, the distance transform was implemented on the inverse of the binary image of the detected retinal blood vessels. Thus, for each pixel of the detected blood vessel, the Euclidean distance of that specific pixel or subject to the nearest border pixels of the blood vessel was computed.

b) After applying the distance transforms, the blood vessel pixels that have the greatest distance values in the distance transform will be located in the middle of the blood vessel segment. The distance values that represent the halfway edge in between the blood vessel segment were obtained with some leniency of the largest distance values because of the floating-point computation.

c) Eventually, the overall average of accumulated distance values defines the half-width of the blood vessel. Consequently, the blood vessel thickness (width) was measured by multiplying the outcome reached by two.
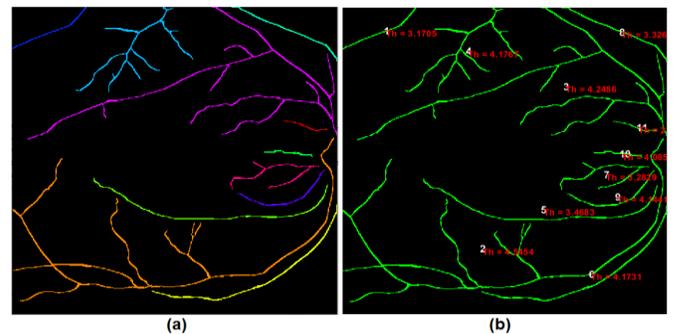
Fig. 7.   The Output of the Developed Thickness Procedure: (a) Coloured Labeled Retinal Blood Vessels and (b) Image Map for the Retinal Blood Vessels along with their Indexes and Average Thickness Values.

IV. EXPERIMENTAL RESULT AND DISCUSSION

In the current research, the accuracy of the developed segmentation approach for recognizing retinal blood vessels was tested using two very difficult fundus image datasets, DRIVE [20] and High-Resolution Fundus (HRF) [21]. These datasets were used to test the method.

Firstly, the main details of the applied retinal image datasets in current experiments are present. Secondly, the evaluation procedure of the fully-automated shrinkage algorithm is given along with their combination and compared their performance among (GT) which represents the ground truth pictures. Finally, the execution of the developed algorithms is compared with the modern approaches.

A. Dataset Precise Description

The execution of the selected blood vessel segmentation algorithms has been tested using two established publicly available datasets of retinal fundus images (DRIVE and HRF). These two datasets have gained special popularity due to they provide the associated GT images, in which the blood vessel is manually detected by different expert observers. Thus, they enable the possibility of comparing the results obtained against the provided GT images to check the reliability and quality of the selected algorithm. The main aim of these two datasets is to establish and encourage comparative studies on developing an automated algorithm for retinal blood receptacles in the fundus pictures.

1) DRIVE dataset [20]: The DRIVE is consisting of 40 colored retinal pictures split into testing and training sets, each one consisting of 20 pictures. A Mask picture that represents the view field (FOV) of the retina area is supplied for each image together with the corresponding GT image. The blood receptacle in the retinal pictures of the training set was manually segmented by one expert. In this work, the training set was used to figure out the elements of the selected segmentation algorithms. On the other hand, the blood vessels in the testing set images were manually segmented by two other experts. The real execution of the proposed receptacle algorithm was assessed using the testing category. DRIVE database contains retinal images captured from several causes of diabetes up to 400 subjects the record starts with age 25 until 90 years old in the Netherlands. Then, 40 images were randomly chosen, 33 images without diabetic retinopathy registered causes and 7th of the images marked in early diabetic retinopathy. Retinal pictures were captured utilizing a Canon machine with a precise model CR5 non-mydriatic 3CCD camera with an angle of 45° as a field of view. All the images were saved in a specific size which is (768 × 584). As an instance of retinal internal photographs from DRIVE dataset responding manually gold standard images are shown in Fig. 8.

2) HRF dataset [21]: The HRF dataset has 45 pictures taken by three different groups, such as healthy people, people with diabetic retinopathy, and people with glaucoma.

3) Each group has 15 pictures utilizing a mydriatic fundus camera with precise model CANON CF-60UVi with angle 60° as field of view. All the images were saved in JPEG format with 24-bits coloured image. Binary field of view mask pictures of the provided dataset in order to perform the analysis only in the region surrounded by the dark background [see Fig. 9(b)]. In this dataset, the tree of blood vessels was manually traced by several experts in the domain of retinal picture interpretation. For instance, retinal internal pictures from HRF dataset images are shown in Fig. 9.

B. Blood Vessel Segmentation Evaluation

In the binary classification task, every single pixel in the input picture is identified as a blood receptacle by the proposed algorithm. In addition to classified as a blood receptacle in the GT image is computed as a (TP) true positive. Moreover, every single pixel is identified as a blood receptacle in the final segmented picture, yet not in the to the ground truth picture is computed as a (FP) false positive. In the evaluation of the retinal vessel segmentation, the average values of five quantitative performance measures were computed to experiment the quality of the selected algorithms, including the Acc., Sen., Spe., PPV, and NPV. These five quantitative measures are computed as follows:

$$Accuracy\ (Acc.) = \frac{TP+TN}{TP+FN+TN+FP} \tag{19}$$

$$Sensitivity\ (Sen.) = \frac{TP}{TP+FN} \tag{20}$$

$$Specificity\ (Spe.) = \frac{TN}{TN+FP} \tag{21}$$

$$Positive\ Predictive\ Value\ (PPV) = \frac{TP}{TP+FP} \tag{22}$$

$$Negative\ Predictive\ Value\ (NPV) = \frac{TN}{TN+FN} \tag{23}$$
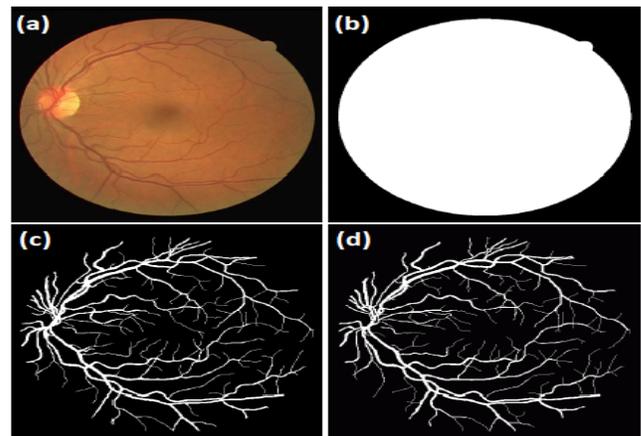
Fig. 8. Image Example from the DRIVE Dataset: (a) The Main Picture, (b) FOV-mask Picture, (c) The Manually Segmented Picture of the First Expert, and (d) Manually Segmented Picture of the Second Expert.

Fig. 9. Image Example from the HRF Dataset: (a) The Main Photograph, (b) FOV-mask Photograph, and (c) The Manually Segmented Photograph of Expert.

Here, the FN, FP, TN, and TP are referring to False Negatives, False Positives, True Negatives, and True Positives sequentially. Acc. measurement is referring to the average of the total amount of correctly identified pixels among to the number of pixels that located in the field of view mask picture. Sen. relates to the selected algorithm's ability to recognise the blood receptacle pixels accurately. Spe. is the capacity of the suggested method to recognise non-vessel pixels accurately.

The positive prediction value is referring to the pixels' average correctly classified as vessel pixels. Finally, the negative prediction value is the pixels average to correctly identified as non-blood receptacle pixels (e.g., background).

C. 4.3. Results on Drive Dataset

Firstly, the execution of the selected algorithm for detecting the retinal blood receptacle was checked out based on the DRIVE dataset. Using training group pictures, several executions were done in field to choose the best value for a group of parameters in order to maximize the segmentation quality of the proposed algorithms. For instance, using the proposed morphological filtering algorithm, the (λ) and (t) parameters values are determined to 0.20 and 5, respectively. The 2D Gaussian filter size was set to (7×7) pixels, values of the low threshold (TL) and the high threshold (TH) were set to 25 and 40, respectively. Then, the segmentation accuracy was computed to select the best value of the parameter (t). So, 121 tests were done where the parameter (t) was changed each time by 0.1.

As shown in Fig. 10, the best value of the parameter (t) was set to 0.5. In the evaluation stage, five performance evaluation metrics were computed using the testing images along with the two provided human observers as the GT images.

The adopted five evaluation metrics using the proposed morphological filtering algorithm are shown in Table IV. Using the two provided human observers as the GT images in the DRIVE dataset the proposed morphological filtering algorithm has managed to achieve an overall average Acc. of 98.06%, Sen. of 97.995%, Spe. of 97.775%, PPV of 90.07%, and NPV of 94.725%. Form Table I, although the proposed morphological filtering algorithm has obtained a higher Spe. of 98.32% using the 1st human observer compared to Spe. of 97.23% using the 2nd human observer, better results were obtained using the letter in terms of other evaluation metrics. Then, the proposed blood vessel linking procedure was applied to correctly join the discontinuous blood vessels produced in the segmented retinal image resulting from the previous step. In this work, to validate the advantage of applying the proposed blood vessel linking procedure, the adopted five evaluation metrics were computed with and without the applying the proposed blood vessel linking procedure. An example of the output segmentation results on the DRVIE dataset is shown in Fig. 11.

In this work, On the images that come from DRIVE group dataset, the execution of the suggested algorithms was compared with modern methods for separating blood vessels.
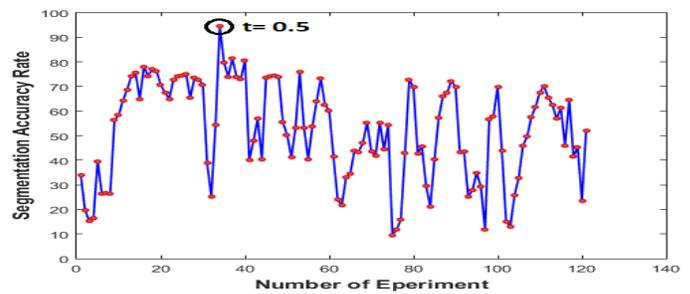
Fig. 10. The Segmentation Accuracy Obtained during 121 Experiments to Fine the Best Value of the Parameter (t) in the using the Proposed Morphological Algorithm.

TABLE I. THE AVERAGE VALUES OF FIVE QUANTITATIVE PERFORMANCE MEASURES USING THE PROPOSED MORPHOLOGICAL FILTERING ALGORITHM ON DRIVE DATASET

Measurements	1st Observer	2nd Observer	Average
Acc.	97.34	98.78	98.06
Sen.	97.67	98.32	97.995
Spe.	98.32	97.23	97.775
PPV	89.92	90.22	90.07
NPV	93.89	95.56	94.725
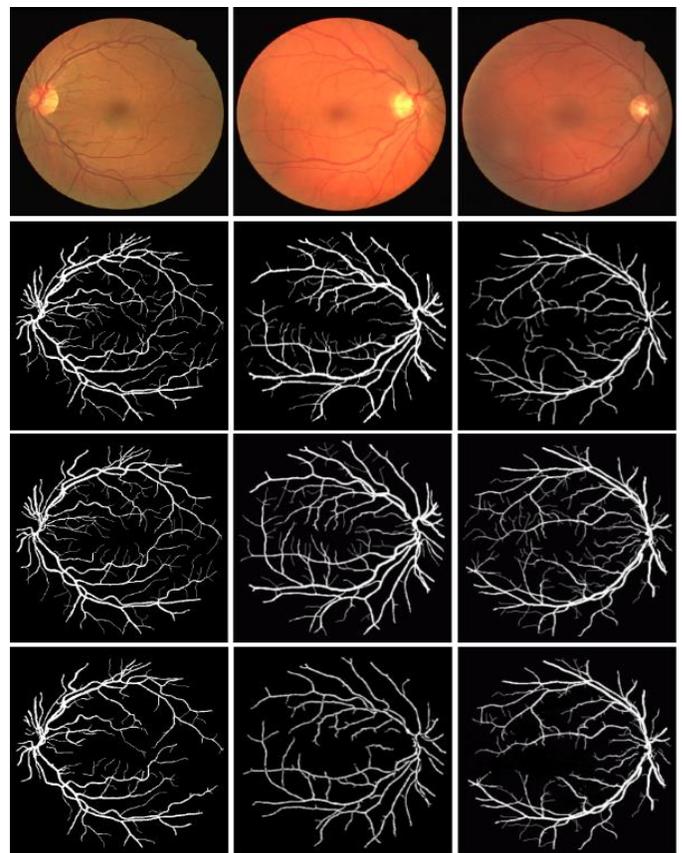
Fig. 11. The Output Segmentation Results in the DRVIE Dataset: The main Picture, The 1st Human Observer Picture, The 2nd Human Observer, and The Output Segmented Picture of the Proposed Morphological Algorithm.

Herein, the results obtained on the 2nd human observer have been considered for comparison purposes. It has been noted that most previously published approaches in the literature are reporting the values of Acc., Sen., and Spe. Thus, the overall average of these three metrics along with the PPV and NPV values have been computed with GT images (2nd human observer) and listed in Table II. Although, Li and his team. [22], Jin. [23], Hassan. [24], Dasgupta and Singh [26], Tamim. [30], and Yang. [28] have achieved a higher Spe. and NPV value compared with the proposed morphological filtering algorithm, they achieved inferior results on the other metrics.

evaluation metrics, for instance, Sensitivity, Specificity, positive prediction value, and negative predictive value which were compared with the proposed morphological filtering algorithm. On the other hand, Chalakkal et al. [35] have achieved a slightly better Spe. value of 100% compared with a Spe. value of 99.17%, 99.35%, and 99.78%, using the morphological filtering algorithm, respectively. However, they got inferior results on the other evaluation matric (e.g., Acc. and Sen.). Finally, one can see the best Sen. value of 98.87%, 99.12%, and 99.89% has been obtained using the morphological filtering algorithm, respectively, the outcome results compared with the modern approaches to HRF dataset.

TABLE II.   EXECUTION RESULTS OF THE COMPARISON OF THE PROPOSED ALGORITHM WITH THE MODERN VESSEL SEGMENTATION APPROACH ON THE DRIVE DATASET

Approaches	Acc.	Sen.	Spe.	PPV	NPV
Odstrcilik et al. [21]	94.73	78.07	97.12	-	-
Li et al. [22]	95.27	75.69	98.16	-	-
Jin et al. [23]	96.97	78.94	98.70	85.37	-
Hassan et al. [24]	96.25	87.99	97.99	-	-
C. Argyrois [25]	94.79	85.06	95.82	-	-
Dasgupta and Singh [26]	95.33	76.91	98.01	84.98	-
Samuel and Veeramalai [27]	96	82	97	-	-
Yang et al. [28]	95.83	73.93	97.92	77.70	97.53
Kishorea and Ananthamoorthy [29]	94.1	69.9	95.8	85.5	94.8
Tamim et al. [30]	96.07	75.42	98.43	86.34	96.53
Yang et al. [31]	95.22	71.81	97.47	89.23	98.5
Yang et al. [32]	94.21	75.60	96.96	78.54	96.44
Keerthiveena et al. [33]	94.71	92.7	95.6	92.49	95.7
Morphological Filtering Algo.	98.78	98.32	97.23	90.22	95.56

D. 4.4 Result of HRF Dataset

The execution of the selected vessels segmentation algorithm has been assessed using HRF dataset using the same parameters configuration described in Section II.2. Initially, the adopted five evaluation metrics have been calculated to the selected vessel shrink algorithms utilizing the GT pictures provided in the HRF dataset, as shown in Table III. It has been noted that a comparable performance has been achieved with the proposed morphological filtering where a PPV of 96.88% and NPV of 100% have been obtained using the proposed morphological filtering algorithm. An example of the output segmentation results for the HRF dataset group is presented in Fig. 12.

The execution of the selected blood vessel segmentation algorithms has also been compared with the modern approaches to the HRF group, as given in Table IV. It has been observed that some existing approaches have achieved slightly higher segmentation accuracy compared with the proposed algorithms. For instance, Kishorea and Ananthamoorthy [29] have reached an Acc. of 99.6% compared to an Acc. of 98.76% and 98.78 using the proposed morphological filtering algorithm. However, the work presented in [32] has obtained inferior results in terms of other

TABLE III.   EXECUTION COMPARISON OF THE SELECTED ALGORITHMS ON THE HRF DATASET

Measurements	Morphological Filtering Algo.
Acc.	98.76
Sen.	98.87
Spe.	99.17
PPV	96.88
NPV	100

Fig. 12. The Output Segmentation Outcomes on the HRF Group: The main Photograph, The Human Observer Photograph, and The Output Segmented Photograph of the Selected Morphological Filtering.

TABLE IV.   EXECUTION COMPARISON OF THE SELECTED ALGORITHMS WITH MODERN BLOOD RECEPTACLE SHRINK APPROACHES ON THE HRF GROUP

Approaches	Acc.	Sen.	Spe.	PPV	NPV
Vostatek [34]	94.3	58.3	97.8	-	-
Kishorea and Ananthamoorthy [29]	99.6	76.52	98.5	87.9	96
Yang [32]	95.17	79.15	96.76	70.79	97.90
Chalakkal [35]	94.4	88.8	100		
Yang [36]	95.49	72.65	97.40	70.03	97.71
Wang [37]	96.54	78.03	98.43	-	-
Khan [38]	95.9	77.2	97.8	-	-
Upadhyay [39]	95.2	75	97.2	72.7	-
Guo and Peng [40]	98.56	80.25	98.54	-	-
Morphological Filtering Algo.	**98.76**	**98.87**	**99.17**	**96.88**	**100**

E. 4.5. Clinical Feature Evaluation

In this section, a medical valuation process was conducted to accurately evaluate the efficiency in addition to the reliability of the proposed algorithms in terms of extracting helpful medical features. These clinical features include the tortuosity, length, density, and thickness of the blood vessel, which are efficiently used to detect several ophthalmological diseases. In the conducted experiments, the automated estimations of the four clinical features were calculated by utilizing the definition of the clinical feature on GT pictures in the adopted datasets.

Initially, the automated estimation of the clinical features from the DRIVE dataset using the 1st human observer was computed by the proposed algorithms and directly compared with the reference values generated from the GT images of the 1st human observer. The overall average (AV.), Standard Deviation (STD), Maximum (Max), and Minimum (Min) of each clinical feature on manual in addition to automated generated pictures. Moreover, (Diff) represents the Difference and (Diff %) represents the percentage difference between both of them which are presented in Table V. The overall average of (Diff%) between the manual shrinkage method and automated using the proposed morphological filtering algorithm was less than 19%, 16.5%, 10%, and 18% for the tortuosity, thickness, length, and density, respectively.

TABLE V. EXECUTION COMPARISON WAS CONDUCTED BETWEEN THE MANUAL SHRINKAGE METHOD AND AUTOMATED ESTIMATIONS OF FOUR CLINICAL FEATURES UTILIZING THE 1ST HUMAN OBSERVER OF DRIVE DATASET

	Manual	**Morphological Filtering**		
	TC	TC	Diff	Diff %
AV.	1.814	1.5015	0.312	18.85
STD	0.8628	0.7877	0.075	9.095
Max	3.78	3.68	0.1	2.680
Min	1.06	1.02	0.04	3.846
	Thick.	Thick.	Diff	Diff %
AV.	3.7735	3.2015	0.572	16.401
STD	0.3722	0.2796	0.092	28.413
Max	4.32	3.72	0.6	14.925
Min	2.98	2.75	0.23	8.02
	NL	NL	Diff	Diff %
AV.	33.447	36.934	-3.48	9.910
STD	4.5592	6.8644	-2.30	40.363
Max	47.48	53.46	-5.98	11.848
Min	28.83	23.89	4.94	18.740
	ND	ND	Diff	Diff %
AV.	0.0129	0.0108	0.002	17.884
STD	0.0103	0.0092	0.001	10.805
Max	0.0343	0.0261	0.008	27.152
Min	0.0025	0.0017	0.0008	38.095

Using the 1st human observer of DRIVE dataset, Pearson correlation plots were also adopted to further confirm the clinical reliability and usefulness of the proposed blood vessel segmentation algorithms as effective tools to provide a precise and automated estimation of the vessel's clinical features. As shown in Fig. 13, the proposed morphological filtering algorithm has managed to achieve (r) representing Pearson's correlation and (p) representing coefficient of: (r = 0.86, p < 0.0001) for vessel tortuosity, (r = 0.86, p < 0.0001) for vessel thickness, (r = 0.79, p < 0.0001) for vessel length, and (r = 0.91, p < 0.0001) for vessel density.
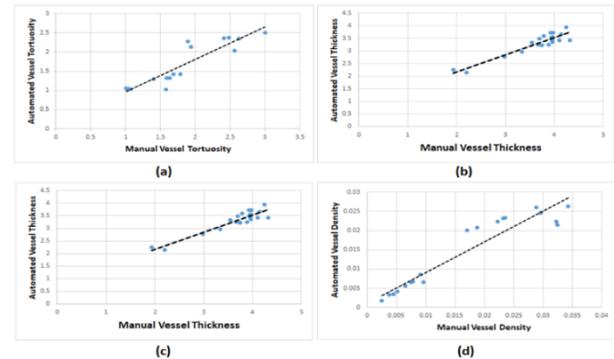
Fig. 13. Correlation Plots between Manual using the 1st Human Observer and Automated Clinical Estimations for the DRIVE Dataset using the Proposed Morphological Filtering Algorithm: (a) Tortuosity, (b) Thickness, (c) Length, and (d) Density. The Same Clinical Evaluation was Carried Out to Get the Automated Estimation of the Clinical Features from the DRIVE Dataset using the 2nd Human Observer.

Fig. 14 and Table VI presents the selected morphological filtering has managed to achieve (R) and (P) with the scale of : (r = 0.94, p < 0.0001) for vessel tortuosity, (r = 0.86, p < 0.0001) for vessel thickness, (r = 0.89, p < 0.0001) for vessel length, and (r = 0.76, p < 0.0001) for vessel density.

TABLE VI. EXECUTION COMPARISON WAS CONDUCTED BETWEEN THE MANUAL SHRINKAGE METHOD AND AUTOMATED METHODS OF FOUR CLINICAL FEATURES UTILIZING THE 2ND HUMAN OBSERVER OF DRIVE DATASET

	Manual	**Morphological Filtering**		
	TC	TC	Diff	Diff %
Average	1.708	1.5015	0.206	12.868
STD	0.903	0.7877	0.116	13.733
Max	4.48	3.68	0.8	19.607
Min	1.01	1.02	-0.01	0.985
	Thick.	Thick.	Diff	Diff %
Average	3.834	3.2015	0.633	17.993
STD	0.378	0.2796	0.099	30.123
Max	4.3	3.72	0.58	14.463
Min	3.12	2.75	0.37	12.606
	NL	NL	Diff	Diff %
Average	33.543	36.934	-3.391	9.622
STD	5.496	6.8644	-1.368	22.145
Max	46.94	53.46	-6.52	12.988
Min	26	23.89	2.11	8.454
	ND	ND	Diff	Diff %
Average	0.013	0.0108	0.0024	20.6010
STD	0.007	0.0092	-0.0017	20.233
Max	0.0344	0.0261	0.0083	27.430
Min	0.0013	0.0017	-0.0004	26.666
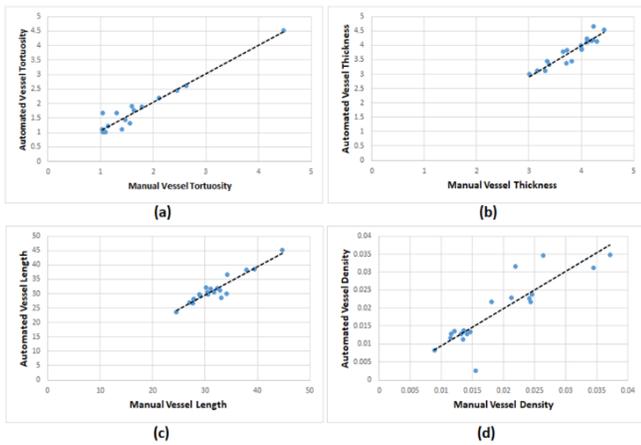
Fig. 14. Correlation Plots between Manual using the 2nd Human Observer and Automated Clinical Estimations for the DRIVE Dataset using the Proposed Morphological Filtering Algorithm: (a) Tortuosity, (b) Thickness, (c) Length, and (d) Density.

TABLE VII. EXECUTION COMPARISON WAS CONDUCTED BETWEEN THE MANUAL SHRINKAGE METHOD AND AUTOMATED METHODS OF FOUR CLINICAL FEATURES UTILIZING HRF DATASET

	Manual	Morphological Filtering		
	TC	TC	Diff	Diff %
Average	1.580	1.5111	0.069	4.485
STD	0.843	0.906	-0.062	7.196
Max	5.38	4.3	1.08	22.314
Min	1.02	1.02	0	0
	Thick.	Thick.	Diff	Diff %
Average	3.834	3.380	0.454	12.584
STD	0.592	0.557	0.034	6.033
Max	5.79	4.98	0.81	15.041
Min	2.67	2.44	0.23	9.001
	NL	NL	Diff	Diff %
Average	28.983	27.949	1.034	3.632
STD	3.673	4.302	-0.628	15.750
Max	38.43	39.73	-1.3	3.326
Min	23.56	20.17	3.39	15.504
	ND	ND	Diff	Diff %
Average	0.0059	0.0054	0.0005	10.087
STD	0.0035	0.0031	0.0003	10.240
Max	0.0189	0.0189	0	0
Min	0.0014	0.0011	0.0002	20.472

The evaluation process is an important task to validate the proposed algorithm and has been used in many studies, such as [29-32]. Further evaluation was performed on HRF Dataset which contains 40 GT images to assess the performance of the selected blood vessel shrinking algorithms. As shown in Table VII, the overall Min, AV, Max, and STD of every clinical feature for the automated and manual pictures were computed along with the Diff and Diff % between them. The average Diff% between manual and automated estimations calculated

using the proposed morphological filtering algorithm was 4.485% v 2.560%, 12.584% v 12.59%, 3.632% v 2.484%, and 10.087% v 5.529% for the tortuosity, thickness, length, and density, respectively. Correlation plots between manual and automated clinical estimations for the HRF dataset using the proposed morphological filtering algorithm are presented in Fig. 15.
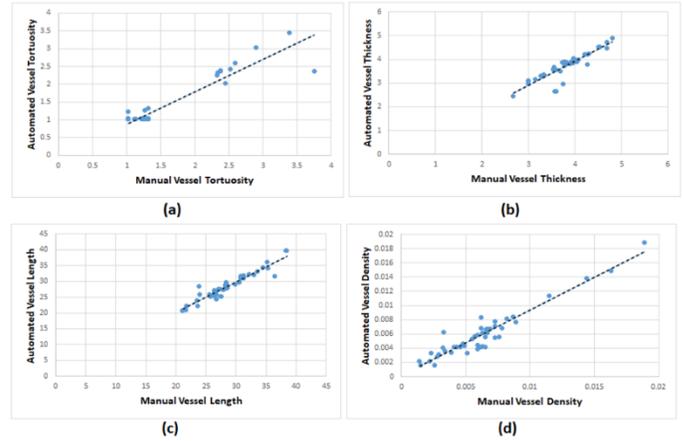
Fig. 15. Correlation Plots between Manual and Automated Clinical Estimations for the HRF Dataset using the Proposed Morphological Filtering Algorithm: (a) Tortuosity, (b) Thickness, (c) Length, and (d) Density.

V. CONCLUSION

In this study, a precise, quick, and fully-automatic blood vessel shrinking in addition to the clinical feature measuring system for retinal fundus images is presented. The proposed morphology has two main steps: separating the blood vessels and pulling out the clinical features. In the blood vessels segmentation stage, a fully-automated segmentation algorithm was proposed and named as a morphological filtering algorithm to classify the blood receptacles in the retinal internal pictures. The algorithm has its own image enhancement procedure which is addressed by pre-processing stage in order to figure out the problems of blurring, variation levels of the light, and poor contrast of the retinal internal picture, plus to promote the early diagnosis of several eye pathologies. Several exhaustive experiments were purely conducted to evaluate the efficacy of the developed fully-automated shrinking algorithm in classified retinal blood receptacles using the DRIVE and HRF datasets of exceedingly demanding fundus images. Initially, the accuracy of the created algorithm was tested based on its ability to accurately recognize retinal blood receptacles. Five quantitative performance measures were computed to validate the efficacy of the selected algorithm, including the accuracy, sensitivity, specificity, positive predictive value, and negative predictive value of 98.78%, 98.32%, 97.23%, 90.22% and 95.56%. According to the HRF dataset results are based on five quantitative performance measures 98.76%, 98.87%, 99.17%, 96.88%, and 100% respectively. Then, the efficiency and reliability of the proposed algorithm in terms of extracting useful and helpful clinical features were also evaluated by conducting a set of extensive experiments. Statistically notable correlations between the manual and automated estimations of the adopted four clinical features have been obtained using the proposed algorithm on both datasets (DRIVE and HRF).

REFERENCES

[1] A. A. Abdulsahib1, M. A. Mahmoud, Mazin Abed Mohammed, Hind Hameed Rasheed, S. A. Mostafa4, and M. S. Maashi, Comprehensive Review of Retinal Blood Vessels Segmentation and Classification Techniques Intelligent Solutions for Green Computing in Medical Images, Current Challenges, Open issues, and Knowledge Gaps in Fundus Medical Images. Network Modeling Analysis in Health Informatics and Bioinformatics (2021) 10:20 https://doi.org/10.1007/s13721-021-00294-7, vol. springer, 2021.

[2] S. Lal, S. U. Rehman, J. H. Shah, T. Meraj, H. T. Rauf, R. Damasevicius, et al.,Adversarial Attack and Defence through Adversarial Training and Feature Fusion for Diabetic Retinopathy Recognition, Sensors (Basel), vol. 21, Jun 7 2021.

[3] K. Balasubramanian and N. P. Ananthamoorthy, Robust retinal blood vessel segmentation using convolutional neural network and support vector machine, Journal of Ambient Intelligence and Humanized Computing, vol. 12, pp. 3559-3569, 2019.

[4] H. Boudegga, Y. Elloumi, M. Akil, M. Hedi Bedoui, R. Kachouri, and A. B. Abdallah, Fast and efficient retinal blood vessel segmentation method based on deep learning network, Comput Med Imaging Graph, vol. 90, p. 101902, Jun 2021.

[5] O. Ramos-Soto, E. Rodriguez-Esparza, S. E. Balderas-Mata, D. Oliva, A. E. Hassanien, R. K. Meleppat, et al., An efficient retinal blood vessel segmentation in eye fundus images by using optimized top-hat and homomorphic filtering,Comput Methods Programs Biomed, vol. 201, p. 105949, Apr 2021.

[6] A. A. Abdulsahib, M. A. Mahmoud, H. Aris, S. S. Gunasekaran, and M. A. Mohammed, An Automated Image Segmentation and Useful Feature Extraction Algorithm for Retinal Blood Vessels in Fundus Images," Electronics, vol. 11, p. 1295, 2022.

[7] M. Z. S. M. L. Jadhav, and V. M. Sardar, "Automated Microaneurysms Detection in Fundus Images for Early Diagnosis of Diabetic Retinopathy, under exclusive license to Springer Nature Singapore Pte Ltd. 2021 V. Bhateja et al. (eds.), Data Engineering and Intelligent Computing, Advances in Intelligent Systems and Computing 1, https://doi.org/10.1007/978-981-16-0171-2_9, 2021.

[8] S. G. G. S. S. Anand, Optic disc analysis in retinal fundus using L2 norm of contourlet subbands, superimposed edges, and morphological filling,Springer, vol. 1210: Computer Vision for Clinical Images Published: 24 October 2021; 2021.

[9] A. S. 2, S. A. 3, P. S. 4, and S. K. B. V, "Retinal Vessel Segmentation Using Morphological Top Hat Approach On Diabetic Retinopathy Images, 978-1-5386-4606-9©2018 IEEE, 2018.

[10] R. Alaguselvi and K. Murugan, "Performance analysis of automated lesion detection of diabetic retinopathy using morphological operation," Signal, Image and Video Processing, vol. 15, pp. 797-805, 2020.

[11] J. Dash and N. Bhoi, Detection of retinal blood vessels from ophthalmoscope images using morphological approach," ELCVIA Electronic Letters on Computer Vision and Image Analysis, vol. 16, p. 1, 2017.

[12] U. Ozkava, S. Ozturk, B. Akdemir, and L. Sevfi, An Efficient Retinal Blood Vessel Segmentation using Morphological Operations, pp. 1-7, 2018.

[13] S. J. a. M. S. Charu Bhardwaj, "Performance analysis of retinal features for diabetic retinopathy characterisation and diagnosis" Published Online:December 15, 2020pp 253-270, 2020.

[14] P. P. A. J. MALIK, Scale-Space and Edge Detection Using Anisotropic Diffusion ,IEEE TRANSACTIONS ON PATTERN ANALYSIS AND MACHINE INTELLIGENCE, VOL. 12. NO. 7. JULY 1990, 1990.

[15] I. D. b and B. C. a. , Buddhajyoti Chattopadhyay a, Enhancing effective depth-of-field by image fusion using mathematical morphology, elsevier, vol. Image and Vision Computing 24 (2006) 1278–1287, 2006.

[16] F. Susanta Mukhopadhyay and Bhabatosh Chanda, IEEE, Multiscale Morphological Segmentation of Gray-Scale Images, IEEE, vol. TRANSACTIONS ON IMAGE PROCESSING, VOL. 12, NO. 5, MAY 2003.

[17] A. S. Al-Waisy, R. Qahwaji, S. Ipson, and S. Al-Fahdawi, A multimodal deep learning framework using local feature representations for face recognition, Machine Vision and Applications, vol. 29, pp. 35-54, 2017.

[18] T. W. J.A. Kylstra l, M.L. Wolbarsht 1' 2, M.B. Landers, III 1, and E. Stefansson The relationship between retinal vessel tortuosity, diameter, and transmural pressure, springer, vol. Graefe's Arch Clin Exp Ophthalmol (1986) 224:477-480, 1986, 1986.

[19] V. M. Martynas Patašius, Arūnas Lukoševičius, Darius Jegelevičius, Model based investigation of retinal vessel tortuosity as a function of blood pressure preliminary results, IEEE, vol. preliminary results Proceedings of the 29th Annual International Conference of the IEEE EMBS Cité Internationale, Lyon, France August 23-26, 2007, 2007.

[20] V. S. Joshi, Analysis of retinal vessel networks using quantitative descriptors OF VASCULAR MORPHOLOGY, the Biomedical Engineering and Bioengineering Commons, 2012.

[21] Jan Odstrcilik1, Radim Kolar1,2, Attila Budai3, J. H. , J. J. , J. G. , , T. Kubena4, et al., "<Retinal vessel segmentation by improved matched filtering: evaluation on a new high-resolution fundus image data., IET, vol. IET Image Process., pp. 1–11 1 doi: 10.1049/iet-ipr.2012.0455, 2013.

[22] M. V. L. Li, Y. Nakashima, H. Nagahara, and R. Kawasaki, IterNet: Retinal image segmentation utilizing structural redundancy in vessel networks, Proc. - 2020 IEEE Winter Conf. Appl. Comput. Vision, WACV 2020, pp. 3645–3654, 2020, doi: 10.1109/WACV45572.2020.9093621.

[23] A. S. A.-W. R. Q. S. I. S. Al-Fahdawi1, A multimodal deep learning framework using local feature representations for face recognition , springer, vol. Machine Vision and Applications DOI 10.1007/s00138-017-0870-2, 2017.

[24] N. E.-B. G. Hassan, A. E. Hassanien, A. Fahmy, S. Abullahm, and V. Snasel, Retinal Blood Vessel Segmentation Approach Based on Mathematical Morphology, Procedia Comput. Sci., vol. 65, no. Iccmit, pp. 612–622, 2015, doi: 10.1016/j.procs.2015.09.005., 2015.

[25] A. C. T. H. Houssem and B. T. F. Cherie, A Multi-scale Tensor Voting Approach for Small Retinal Vessel Segmentation in High Resolution Fundus Images, Comput Med Imaging Graph, 2016. 52: p. 28-43., 2016.

[26] A. Dasgupta and S. Singh, A fully convolutional neural network based structured prediction approach towards the retinal vessel segmentation, Proc. - Int. Symp. Biomed. Imaging, pp. 248–251, 2017, doi: 10.1109/ISBI.2017.7950512., 2017.

[27] P. M. Samuel and T. Veeramalai, Multilevel and multiscale deep neural network for retinal blood vessel segmentation, Symmetry (Basel)., vol. 11, no. 7, 2019, doi: 10.3390/sym11070946., 2019.

[28] F. S. Y. Yang, Z. Fu, and R. Fu, Blood vessel segmentation of fundus images via cross-modality dictionary learning," Appl. Opt., vol. 57, no. 25, p. 7287, 2018, doi: 10.1364/ao.57.007287., 2018.

[29] B. Kishore and N. P. Ananthamoorthy, Glaucoma classification based on intra-class and extra-class discriminative correlation and consensus ensemble classifier, Genomics, vol. 112, no. 5, pp. 3089–3096, 2020, doi: 10.1016/j.ygeno.2020.05.017., 2020.

[30] M. E. Nasser Tamim, Gamil Abdel Azim and Hamed Nassar, Retinal Blood Vessel Segmentation Using Hybrid Features and Multi-Layer Perceptron Neural Networks, MDPI, vol. Symmetry 2020, 12, 894; doi:10.3390/sym12060894, 2020.

[31] M. H. J. Yang, J. Fu, C. Lou, and C. Feng, Frangi based multi-scale level sets for retinal vascular segmentation, Comput. Methods Programs Biomed., vol. 197, p. 105752, 2020, doi: 10.1016/j.cmpb.2020.105752., 2020.

[32] F. S. Y. Yang, Z. Fu, and R. Fu, Discriminative dictionary learning for retinal vessel segmentation using fusion of multiple features, Signal, Image Video Process., vol. 13, no. 8, pp. 1529–1537, 2019, doi: 10.1007/s11760-019-01501-9., 2019.

[33] S. E. B. Keerthiveena, K. Selvakumar, and T. Yogesh, Computer-aided diagnosis of retinal diseases using multidomain feature fusion, Int. J.

Imaging Syst. Technol., vol. 30, no. 2, pp. 367–379, 2020, doi: 10.1002/ima.22379., 2020.

[34] P. Vostatek, Blood Vessel Segmentation in the Analysis of Retinal and Diaphragm Images Blood Vessel Segmentation in the Analysis of Retinal and Diaphragm, 2017.

[35] W. H. A. R. J. Chalakkal, and S. S. Thulaseedharan, Quality and content analysis of fundus images using deep learning, Comput. Biol. Med., vol. 108, no. March, pp. 317–331, 2019, doi: 10.1016/j.compbiomed.2019.03.019., 2019.

[36] X. Y. Z. Yan, and K. T. Cheng, Joint segment-level and pixel-wise losses for deep learning based retinal vessel segmentation, IEEE Trans. Biomed. Eng., vol. 65, no. 9, pp. 1912–1923, 2018, doi: 10.1109/TBME.2018.2828137.

[37] A. H. D. Wang, J. Pottenburgh, O. Saeedi, and Y. Tao, Hard Attention Net for Automatic Retinal Vessel Segmentation, IEEE J. Biomed. Heal. Informatics, vol. 24, no. 12, pp. 3384–3396, 2020, doi: 10.1109/JBHI.2020.3002985., 2020.

[38] M. S. S. K. B. Khan, M. Ahmad, and M. Mazzara, A Hybrid Unsupervised Approach for Retinal Vessel Segmentation, Biomed Res. Int., vol. 2020, doi: 10.1155/2020/8365783., 2020.

[39] M. A. K. Upadhyay, and P. Vashist, Unsupervised multiscale retinal blood vessel segmentation using fundus images, IET Image Process., vol. 14, no. 11, pp. 2616–2625, 2020, doi: 10.1049/iet-ipr.2019.0969., 2020.

[40] Y. Guo and Y. Peng, BSCN: Bidirectional symmetric cascade network for retinal vessel segmentation, BMC Med. Imaging, vol. 20, no. 1, pp. 1–22, 2020, doi: 10.1186/s12880-020-0412-7., 2020.